Substituent-Induced Perturbation Symmetries and Distortions of *meso-tert*-Butylporphyrins

Xing-Zhi Song,[†,‡] Walter Jentzen,[†,§] Laurent Jaquinod,[||] Richard G. Khoury,[||] Craig J. Medforth,[||] Song-Ling Jia,[†,‡] Jian-Guo Ma,[†,‡] Kevin M. Smith,[||] and John A. Shelnutt*[,†,‡]

Materials Theory and Computation Department, Sandia National Laboratories,[⊥] Albuquerque, New Mexico 87185-1349, Department of Chemistry, University of New Mexico, Albuquerque, New Mexico 87131, Klinik und Poliklinik für Nuklearmedizin, Universität GH Essen, Hufelandstrasse 55, D-45147 Essen, Germany, and Department of Chemistry, University of California, Davis, California 95616

Received September 19, 1997

The out-of-plane and in-plane distortions of a series of nickel(II) meso-substituted porphyrins with 0, 1, 2, or 4 *tert*-butyl groups [nickel(II) porphine (NiP), nickel(II) mono-*tert*-butylporphyrin (NiMtBuP), nickel(II) di-*tert*-butylporphyrin (NiDtBuP), and nickel(II) tetra-*tert*-butylporphyrin (NiTtBuP)] are investigated using molecular mechanics (MM) calculations, X-ray crystallography, UV−visible absorption spectroscopy, and resonance Raman spectroscopy. MM calculations are used to predict the stable conformations for this series of porphyrins. The out-of-plane distortions are then analyzed in terms of displacements along the normal coordinates of the porphyrin macrocycle using a new normal-coordinate structural decomposition method. As expected, the distortions are found to occur primarily along the lowest-frequency normal coordinate of each symmetry type and the distortions could be adequately simulated using only the lowest-frequency normal coordinates as a basis (the minimal basis). However, the distortions could be simulated significantly more accurately by extending the minimal basis by including the second-lowest-frequency normal coordinate of all symmetries. Using the extended basis is most important for the in-plane distortions. Detailed analysis of the types of distortion revealed that both the out-of-plane and the in-plane distortions depend on the perturbation symmetry of the peripheral substituents. The symmetry primarily depends on the pattern of substitution (number and positions of substituents) and the orientations of substituents. Often the perturbation symmetry can be predicted for a given porphyrin simply from the possible orientations of the substituents. Then, the main type(s) of symmetric deformation occurring for each possible molecular symmetry can be readily predicted from a D_{4h} correlation table. The stable conformers predicted by MM for the series of *tert*-butyl-substituted porphyrins confirm this simple but informative approach. Experimental verification of the calculated contributions of the symmetric deformations is provided by normal-coordinate structural decomposition of the available X-ray crystal structures of NiP, NiMtBuP, and NiDtBuP. The solid-state results are also supported by the resonance Raman and UV−visible absorption spectroscopic characterization of the porphyrins in solutions. The X-ray crystal structure of NiMtBuP is reported here for the first time.

Introduction

Significant nonplanar distortions of the porphyrin macrocycle are observed in X-ray crystal structures of most hemoproteins. The heme macrocycle displays a range of distorted nonplanar shapes,[1−4] which are presumably caused by different protein environments surrounding the heme. This presumption is based on evidence showing that the isolated heme group is nearly planar in solution environments and that external forces must be applied to cause significant nonplanar distortion.[5] Recently, a normal-coordinate structural decomposition (NSD) method was developed for characterizing the distortions of the porphyrin macrocycle in terms of displacements along the normal coordinates of the macrocycle.[6] It provides a means of analyzing the complicated structures of heme groups in proteins. Further, NSD of the hemoproteins has revealed that the nonplanar conformation of the heme is typically conserved for proteins which belong to the same functional class.[7] For example, a mainly ruffled (*ruf*) type of nonplanar distortion is conserved for mitochondrial *c*-type cytochromes isolated from different species. This heme structural conservation is even observed in proteins for which there is a large natural variation in the amino

* To whom correspondence should be addressed.
† Sandia National Laboratories.
‡ University of New Mexico.
§ Universität GH Essen.
|| University of California.
⊥ Sandia is a multiprogram laboratory operated by Sandia Corporation, a Lockheed Martin Company, for the United States Department of Energy under Contract DE-AC04-94-AL85000.

(1) Higuchi, Y.; Kusunoki, M.; Matsuura, Y.; Yasuoka, N.; Kakudo, M. *J. Mol. Biol.* **1984**, *172*, 109.
(2) Fermi, G.; Perutz, M. F.; Shaanan, B.; Fourme, R. *J. Mol. Biol.* **1984**, *175*, 159.
(3) Finzel, B. C.; Poulos, T. L.; Kraut, J. *J. Biol. Chem.* **1984**, *259*, 13027. (b) Poulos, T. L.; Finzel, B. C.; Howard A. J. *Biochemistry* **1986**, *25*, 5314.
(4) Louie, G. V.; Brayer, G. D. *J. Mol. Biol.* **1990**, *214*, 527.
(5) Anderson, K. K.; Hobbs, J. D.; Luo, L.; Stanley, K. D.; Quirke, J. M. E.; Shelnutt J. A. *J. Am. Chem. Soc.* **1993**, *115*, 12346.
(6) Jentzen, W.; Song, X.-Z.; Shelnutt, J. A. *J. Phys. Chem. B* **1997**, *101*, 1684.
(7) Shelnutt, J. A.; Song, X.-Z.; Ma, J.-G.; Jia, S.-L.; Jentzen, W.; Medforth, C. J. *Chem. Soc. Rev.* **1998**, 31. (b) Jentzen, W.; Ma, J.-G.; Shelnutt, J. A. *Biophys. J.* **1998**, *74*, 753. (c) Hobbs, J. D.; Shelnutt, J. A. *J. Protein Chem.* **1995**, *14*, 19.

S0020-1669(97)01197-X CCC: $15.00
Published on Web 04/14/1998

acid sequence.[6,7b] This finding strongly suggests a biological function for the nonplanar structures. The possible functional importance of these nonplanar heme structures in proteins has been suggested by several other authors[8−11] and is supported by model studies in which nonplanar distortions have been shown to influence redox potential,[8,9a,12] axial ligation,[9] electron-transfer rates,[9a,13] and photophysical processes.[14−16]

To understand the structure−function relationship in this case, it is necessary to know the mechanisms of distortion of the porphyrin macrocycle, that is, how different nonplanar structures occur and what the protein factors are that control them. Theoretically, the factors that influence the structure of the macrocycle can be classified into one of four basic categories: peripheral substitution, the central metal, axial ligation, and the environment of the heme. Peripheral substitution includes the substitution pattern (the number and sites of substituents), the substituent orientations, and substituent properties (steric shape and size, electronic properties). The central metal may vary in electronic nature and size. The environment may be something as complex as a protein or simply the solvent. Our group has been systematically studying the effects of many of these factors on nonplanar distortions of metalloporphyrins using model systems. The steric effects of substituents have been explored by studying various series of di-,[17] tetra-,[18] and dodeca-substituted[19] porphyrins with different peripheral substituent groups. The metal dependence of nonplanar distortions has been studied by examining series of di-,[20] dodeca-,[21] and other-substituted[22] porphyrins with metals of different sizes. The studies on the electronic properties of substituents have been conducted on the series of dodecaphenylporphyrins with different numbers of halogen atoms on the phenyl groups.[23] Systematic studies of axial ligation on the nonplanar distortions are under way.

In this work, we investigate the effect of the symmetry of the substitution pattern and substituent orientations on the out-of-plane and in-plane distortions of the porphyrin macrocycle. A series of nickel porphyrins with 0, 1, 2, and 4 *meso*-*tert*-butyl groups [nickel(II) porphine (NiP), nickel(II) mono-*tert*-butylporphyrin (NiMtBuP), nickel(II) di-*tert*-butylporphyrin (NiDtBuP), and nickel(II) tetra-*tert*-butylporphyrin (NiTtBuP)] were studied using molecular mechanics (MM) calculations, X-ray crystallography, UV−visible absorption spectroscopy, and resonance Raman spectroscopy. MM calculations have previously been used by several other groups[24,25] to predict the conformations of metalloporphyrins. The force field employed here has been shown to be capable of accurately predicting the possible structures of metalloporphyrins that can appear in crystals.[17,20] Here, the conformers predicted by MM are compared with the available X-ray crystal structures for the series of porphyrins, including the crystal structure of NiMtBuP determined in this study. The comparison is facilitated by characterization of the structures using the new normal-coordinate structural decomposition method.[6,7b] As before, we found that the distortions primarily occur along the collection of lowest-frequency normal coordinates of the macrocycle that includes one mode of each symmetry type. Further, as is expected, the types of distortion (both in-plane and out-of-plane) for a specific porphyrin depend on the perturbation symmetry introduced by the peripheral substituents. Surprisingly simple symmetry and energy arguments lead to *a priori* predictions of the perturbation symmetry and thus the types of stable conformers that are possible for a given porphyrin. Similar reasoning gives novel insights into the distortion mechanisms of hemes in proteins. The predicted degree of nonplanar distortions for the series of porphyrins is confirmed by comparison of the NSD results for the calculated and X-ray structures and by UV−visible absorption and resonance Raman spectroscopies of the porphyrin in solution.

Materials and Methods

Synthesis. The synthesis of 5,15-di-*tert*-butylporphyrin (H_2DtBuP), 5,10,15,20-tetra-*tert*-butylporphyrin (H_2TtBuP), and the nickel complexes of these porphyrins (NiDtBuP and NiTtBuP) is described

(8) Kratky, C.; Waditschatka, R.; Angst, C.; Johansen, J.; Plaquevent, J. C.; Schreiber, J.; Eschenmoser, A. *Helv. Chim. Acta* **1982**, *68*, 1312. (b) Waditschatka, R.; Kratky, C.; Jaun, B.; Heiner, J.; Eschenmoser, A. *J. Chem. Soc., Chem. Commun.* **1985**, 1604.
(9) Barkigia, K. M.; Chantranupong, L.; Smith, K. M.; Fajer, J. *J. Am. Chem. Soc.* **1988**, *110*, 7566. (b) Furenlid, L. R.; Renner, M. W.; Smith, K. M.; Fajer, J. *J. Am. Chem. Soc.* **1990**, *112*, 1634. (c) Furenlid, L. R.; Renner, M. W.; Smith, K. M.; Fajer, J. *J. Am. Chem. Soc.* **1990**, *112*, 8987. (d) David, S.; James, B. R.; Dolphin, D.; Traylor, T. G.; Lopez, M. A. *J. Am. Chem. Soc.* **1994**, *116*, 6.
(10) Tronrud, D. E.; Schmid, M. F.; Matthews, B. W. *J. Mol. Biol.* **1986**, *188*, 443.
(11) Geno, M. K.; Halpern, A. G. *J. Am. Chem. Soc.* **1987**, *109*, 1238.
(12) Kadish, K. M.; Van Caemelbecke, E.; D'Souza, F. D.; Medforth, C. J.; Smith, K. M.; Tabard, A. *Organometallics* **1993**, *12*, 2411. (b) Kadish, K. M.; Van Caemelbecke, E.; D'Souza, F. D.; Boulas, P.; Vogel, E.; Kisters, M.; Medforth, C. J.; Smith, K. M. *Inorg. Chem.* **1993**, *32*, 4177.
(13) Plato, M.; Mobius, K.; Michel-Beyerle, M. E.: Bixon, M.; Jortner, J. *J. Am. Chem. Soc.* **1988**, *110*, 7279.
(14) Gudowska-Nowak, E.; Newton, M. D.; Fajer, J. *J. Phys. Chem.* **1990**, *94*, 5795.
(15) Medforth, C. J.; Berber, M. D.; Smith, K. M.; Shelnutt, J. A. *Tetrahedron Lett.* **1990**, *31*, 3719.
(16) Shelnutt, J. A.; Medforth, C. J.; Berber, M. D.; Barkigia, K. M.; Smith, K. M. *J. Am. Chem. Soc.* **1991**, *113*, 4077.
(17) Song, X.-Z.: Jentzen, W.; Jia, S.-L.; Jaquinod, L.; Nurco, D. J.; Medforth, C. J.; Smith, K. M.; Shelnutt, J. A. *J. Am. Chem. Soc.* **1996**, *118*, 12975.
(18) Jentzen, W; Simpson, M. C.; Hobbs, J. D.; Song, X.; Ema, T.; Nelson, N. Y.; Medforth, C. J.; Smith, K. M.; Veyrat, M.; Mazzanti, M.; Ramasseul, R.; Marchon, J.-C.; Takeuchi, T.; Goddard, W. A., III; Shelnutt, J. A. *J. Am. Chem. Soc.* **1995**, *117*, 11085.
(19) Medforth, C. J.; Hobbs, J. D.; Rodriguez, M. R.; Abraham, R. J.; Smith, K. M.; Shelnutt, J. A. *Inorg. Chem.* **1995**, *34*, 1333. (b) Miura, M.; Majumder, S. A.; Hobbs, J. D.; Renner, M. W.; Furenlid, L. R.; Shelnutt, J. A. *Inorg. Chem.* **1994**, *33*, 6078. (c) Sparks, L. D.; Anderson, K. K.; Medforth, C. J.; Smith, K. M.; Shelnutt, J. A. *Inorg. Chem.* **1994**, *33*, 2297. (d) Medforth, C. J.; Muzzi, C. M.; Smith, K. M.; Abraham, R. J.; Hobbs, J. D.; Shelnutt, J. A. *J. Chem. Soc., Chem. Commun.* **1994**, 1843. (e) Hobbs, J. D.; Majumder, S. A.; Luo, L.; Sickelsmith, G. A.; Quirke, J. M. E.; Medforth, C. J.; Smith, K. M.; Shelnutt, J. A. *J. Am. Chem. Soc.* **1994**, *116*, 3261. (f) Medforth, C. J.; Senge, M. O.; Smith, K. M.; Sparks, L. D.; Shelnutt, J. A. *J. Am. Chem. Soc.* **1992**, *114*, 9859. (g) Shelnutt, J. A.; Majumder, S. A.; Sparks, L. D.; Hobbs, J. D.; Medforth, C. J.; Senge, M. O.; Smith, K. M.; Miura, M.; Luo, L.; Quirke, J. M. E. *J. Raman Spectrosc.* **1992**, *23*, 523.
(20) Song, X.-Z.; Jaquinod, L.; Jentzen, W.; Nurco, D. J.; Jia, S.-L.; Khoury, R. G.; Ma, J.-G.; Medforth, C. J.; Smith, K. M.; Shelnutt, J. A. *Inorg. Chem.* **1998**, *37*, 2009.
(21) Sparks, L. D.; Medforth, C. J.; Park, M.-S.; Chamberlain, J. R.; Ondrias, M. R.; Senge, M. O.; Smith, K. M.; Shelnutt, J. A. *J. Am. Chem. Soc.* **1993**, *115*, 581.
(22) Sparks, L. D.; Chamberlain, J. R.; Hsu, P.; Ondrias, M. R.; Swanson, B. A.; Ortiz de Montellano, P. R.; Shelnutt, J. A. *Inorg. Chem.* **1993**, *32*, 3153.
(23) Medforth, C. J.; Caemelbeck, E. V.; Forsyth, T. P.; Hobbs, J. D.; Kadish, K. M.; Ma, J.-G.; Nurco, D. J.; Showalter, M.; Simpson, M. C.; Song, X.-Z.; D'Souza, F.; Smith, K. M.; Shelnutt, J. A., in preparation.
(24) Munro, O. Q.; Marques, H. M.; Debrunner, P. G.; Mohanrao, K.; Scheidt, W. R. *J. Am. Chem. Soc.* **1995**, *117*, 935. (b) Munro, O. Q.; Bradley, J. C.; Hancock, R. D.; Marques, H. M.; Marsicana F., *J. Am. Chem. Soc.* **1992**, *114*, 7218. (c) Marques, H. M.; Munro, O. Q.; Grimmer, N. E.; Levendis, D. C.; Marsicana, F.; Pattrick, G.; Markonlides, T. *J. Chem. Soc., Faraday Trans.* **1995**, *91*, 1741.
(25) Kollman, P. A.; Grootenhuis, D. D. J.; Lopez, M. A. *Pure Appl. Chem.* **1989**, *61*, 593. (b) Lopez, M. A.; Kollman, P. A. *J. Am. Chem. Soc.* **1989**, *111*, 6212.

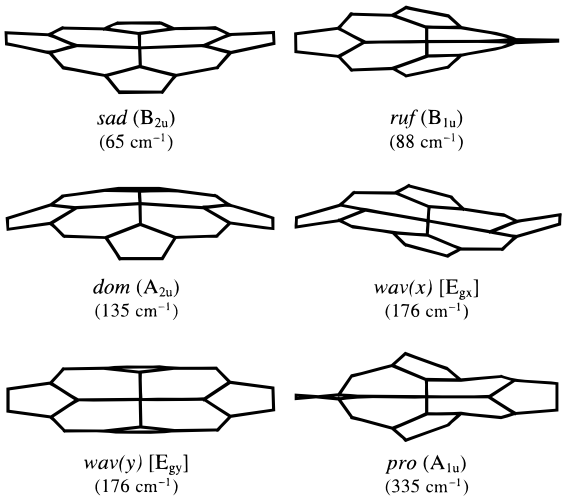

Figure 1. Illustrations of the lowest-frequency out-of-plane eigenvectors, the minimal basis, used for simulating the nonplanar distortions of the porphyrin macrocycle. Static displacements representing a 1-Å deformation along each lowest-frequency normal coordinate are shown.

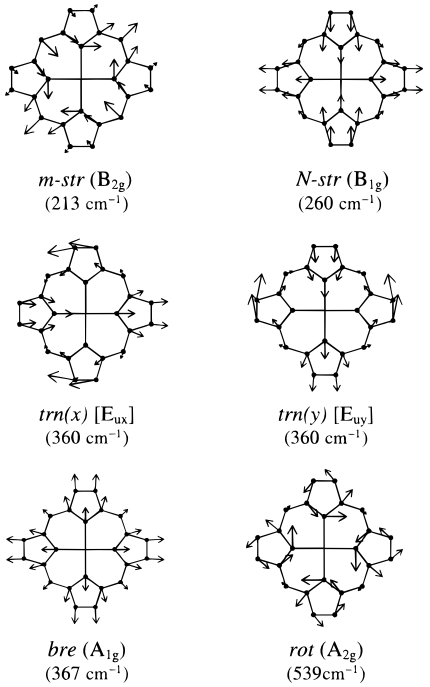

Figure 2. Illustrations of the lowest-frequency in-plane eigenvectors, the minimal basis, used for simulating the in-plane distortions of the porphyrin macrocycle. In-plane displacements represent a 1-Å deformation along each lowest-frequency normal coordinate.

elsewhere.[17,18] 5-*tert*-Butylporphyrin (H_2MtBuP) was obtained in 0.3% yield as a byproduct from the synthesis of H_2DtBuP. Nickel was inserted using the procedure described for NiDtBuP.

H_2MtBuP: mp 230−231 °C; ^{1}H NMR ($CDCl_3$, 300 MHz) δ 10.15 (s, 1H, H_{meso}), 10.06 (s, 2H, H_{meso}), 9.94 (d, 2H, β-H), 9.37 (m, 4H, β-H), 9.28 (d, 2H, β-H), 2.63 (s, 9H, CH_3), −2.64 (s, 2H, NH); MS *m*/*z* 367.2 MH^+ (100).

NiMtBuP: mp >300 °C; ^{1}H NMR ($CDCl_3$, 300 MHz) δ 9.69 (d, 2H, β-H), 9.63 (s, 1H, H_{meso}), 9.52 (s, 2H, H_{meso}), 9.14 (d, 2H, β-H), 9.08 (d, 2H, β-H), 9.01 (d, 2H, β-H), 2.17 (s, 9H, CH_3).

Crystal Structure Determination for NiMtBuP. Crystals of NiMtBuP were grown by slow diffusion of methanol into a solution of the porphyrin in dichloromethane. A single crystal was selected with dimensions of 0.30 × 0.04 × 0.01 mm. The unit cell was orthorhombic *Pbca* with cell dimensions a = 11.9141(13) Å, b = 10.707(2) Å, c = 29.017(4) Å, $\alpha = \beta = \gamma = 90°$, V = 3701.6(9) Å^3, and Z = 8 (fw = 423.15, ρ_{calc} = 1.519 g cm^{-3}, μ = 1.647 mm^{-1}). X-ray diffraction data were collected on a Siemens P4 diffractometer with a rotating anode [λ(Cu Kα) = 1.541 78 Å] at 130(2) K in $\theta/2\theta$ scan mode to $2\theta_{max}$ = 112°. Of the 2823 reflections measured ($\pm h,\pm k,\pm l$), 2419 were independent and 1375 had $I > 2\sigma$ (R_{int} = 0.015). The structure was solved by direct methods and refined (based on F^2 using all independent data) by full-matrix least-squares methods (Siemens SHELXTL version 5.02); the number of parameters was 262. Hydrogen atoms were placed at idealized positions and refined using a riding model. An absorption correction was applied using the program XABS2.[26] Final R factors were R1 = 0.066 (based on observed data) and wR2 = 0.1809 (based on all data).

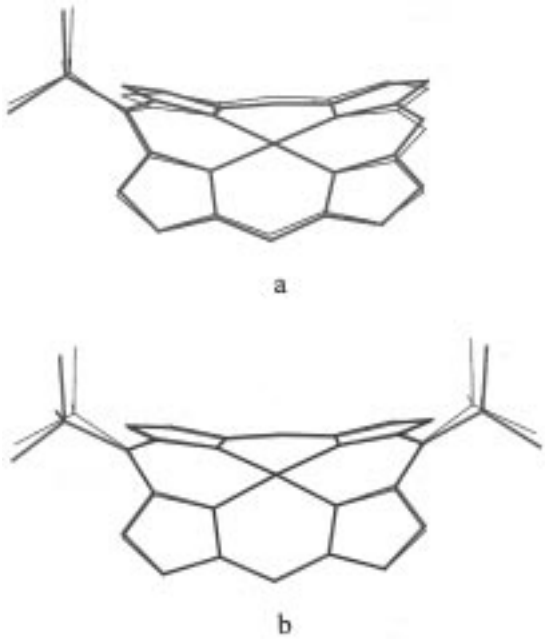

Figure 3. Comparison of the X-ray crystal structure (heavy red line) and the energy-minimized structure (blue line) for NiMtBuP (a) and NiDtBuP (b).

UV−Visible Absorption Spectroscopy. UV−visible absorption spectra were obtained with a 10-mm quartz cell using a HP 8452A diode-array spectrophotometer (Hewlett-Packard). The absorption spectra of the porphyrins were taken in carbon disulfide. The peak positions of the absorption bands were obtained by curve-fitting the absorption spectra with Gaussian lines. The estimated error in the band positions is less than ±1 nm.

Resonance Raman Spectroscopy. Resonance Raman spectra were obtained using a partitioned Raman cell and a dual-channel spectrometer.[27] The 413.1-nm line from a krypton ion laser (Coherent, INNOVA 20) was used for excitation resonant with the Soret band region of the absorption spectrum. The scattered light was collected in the 90° scattering geometry. The porphyrin samples were dissolved in carbon disulfide. Nickel(II) tetraphenylporphyrin (NiTPP) in carbon disulfide was used as reference. The sample and reference solutions were put into a partitioned two-compartment Raman cell. The Raman cell was rotated at 50 Hz to prevent local heating of the sample and to alternately probe the sample and reference solutions, allowing the Raman spectra of the sample and reference to be obtained simultaneously. The typical conditions were 50−60-mW laser power, 5-cm^{-1} spectral slit width, 4−6 scans with 0.3-cm^{-1} increments, and 1-s integration times. The frequency calibrations were carried out by using the ν_4 line of NiTPP in carbon disulfide at 1373.3 cm^{-1} as the reference. The latter was calibrated with the 992.2-, 606.7-, and 1586.4/1606.2-cm^{-1} lines of benzene.[27] In addition, all the spectra were corrected for the nonlinearity

(26) Parkin, S. R.; Moezzi, B.; Hope, H. *J. Appl. Crystallogr*. **1995**, *28*, 53
(27) Shelnutt, J. A. *J. Phys. Chem.* **1983**, *87*, 605.

of the spectrometer. The accuracy of the cited frequencies is ± 1 cm^{-1} with greater accuracy for the differences between spectra run simultaneously.[28]

Molecular Mechanics Calculations. Molecular energy-optimization calculations were carried out using POLYGRAF software (Molecular Simulations, Inc.) and displayed on a Silicon Graphics workstation. The original force field used in the calculations has been described elsewhere[29] as have the subsequent improvements.[17,18,19e,22] It is a hybrid force field based on the DREIDING II parameters[30] modified to include atom types specific to the porphyrin macrocycle. Force constants for the macrocycle atom types were obtained from the normal-coordinate analyses of nickel porphyrins.[31] The equilibrium bond lengths and bond angles were then varied to obtain the closest match of the energy-optimized structure of nickel(II) octaethylporphyrin (NiOEP) with the planar crystal structures of NiOEP.[32,33] Most importantly, a recent significant improvement was made by a 50% reduction of the out-of-plane force constants.[17] This improvement corrected in an approximate manner a long-existing problem, namely, the contribution of the in-plane force constants to the independently obtained out-of-plane force constants. This improvement also makes the force field capable of accurately predicting the structures of various conformers and their relative energies.[20,34]

Normal-Coordinate Structural Decomposition. NSD is a method recently developed by our group for classifying and quantifying the out-of-plane and in-plane distortions of the porphyrin macrocycle.[6,7b] It characterizes the distortion in terms of equivalent displacements along the normal coordinates of the D_{4h} symmetric porphyrin macrocycle. Theoretically, the complete set of $3N - 6$ (=66) normal coordinates forms a basis for exactly describing all possible distortions of the 24 macrocyclic atoms. For the D_{4h} symmetric macrocycle, the basis can be divided into two independent subsets: the out-of-plane (OOP) basis set that consists of the $N - 3 = 21$ normal modes of the out-of-plane symmetry types (3 B_{2u}, 3 B_{1u}, 3 A_{2u}, 5 E_g, and 2 A_{1u}) and the in-plane (IP) basis that consists of the $2N - 3 = 45$ normal modes of the in-plane symmetry types (6 B_{2g}, 6 B_{1g}, 11 E_u, 6 A_{1g}, and 5 A_{2g}). Any distortion from planar geometry can be exactly represented or simulated by a linear combination of all the OOP normal coordinates, and any IP distortion from the ideal reference geometry, which is chosen to be copper(II) porphine,[6] can be described or simulated by a linear combination of all the IP normal coordinates. The linear coefficients are obtained by the NSD mathematical procedure, which projects out the distortion along each of the normal coordinates.[6,7b]

The NSD method is an alternative to giving the *x*, *y*, and *z* displacements for each atom of the porphyrin skeleton. The advantage of a description in terms of the normal coordinates is that the distortion energy of the macrocycle takes on its simplest form in the normal mode representation.[6,7b,17] For any actual distortion, a great simplification in the description occurs because the distortion of the porphyrin will generally take place along only the lowest-frequency normal coordinates since the restoring forces are the smallest for displacements along these coordinates. In fact, using only the set composed of the lowest-frequency normal coordinate of each symmetry type (the *minimal* basis set) usually well simulates the distortion of the porphyrin macrocycle. The minimal basis, as illustrated in Figures 1 and 2, consists of ruffling (*ruf*, B_{1u}), saddling (*sad*, B_{2u}), doming (*dom*, A_{2u}), waving (*x*, *y*) [*wav*(*x*), *wav*(*y*); E_{gx}, E_{gy}], and propellering (*pro*, A_{1u}) for OOP distortions and meso-stretching (*m-str*, B_{2g}), nitrogen stretching (*N-str*, B_{1g}), *x*-translation [*trn*(*x*), E_{ux}], *y*-translation [*trn*(*y*), E_{uy}], breathing (*bre*, A_{1g}), and pyrrole rotation (*rot*, A_{2g}) for IP distortions. The structures shown in Figures 1 and 2 illustrate 1-Å deformations along each of the normal coordinates (normal deformations). That is, the square root of the sum of the squares of the displacements is equal to 1 Å for each of the structures shown.

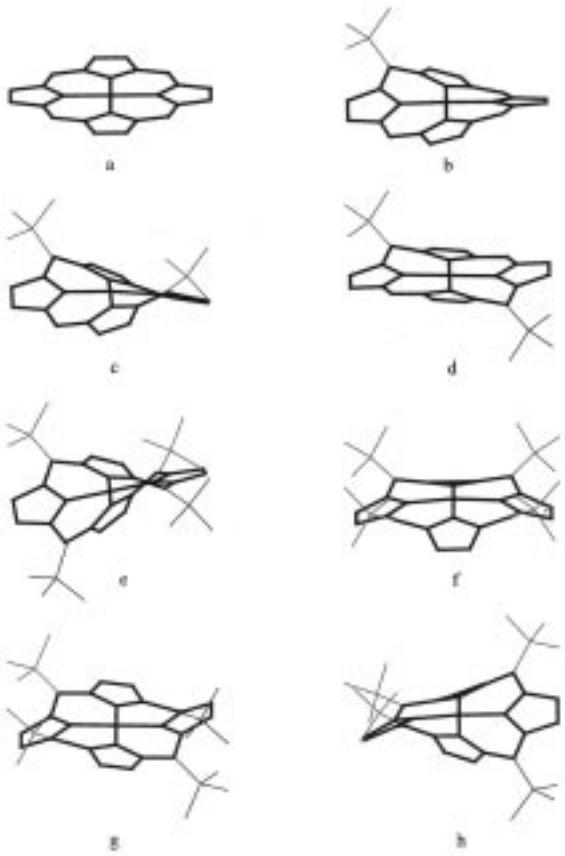

Figure 4. The energy-minimized stable conformers for the series of nickel porphyrins with different numbers of *meso-tert*-butyl substituents. The conformations are obtained from different starting orientations of the substituents: (a) NiP, (b) α-NiMtBuP, (c) αα-NiDtBuP, (d) α*β*-NiDtBuP, (e) α*β*α*β*-NiTtBuP, (f) αααα-NiTtBuP, (g) αα*ββ*-NiTtBuP, (h) ααα*β*-NiTtBuP.

The minimal basis is usually adequate for simulating the structures of porphyrins found in X-ray structures of proteins. However, for accurate simulation of the macrocyclic distortions of the high-resolution structures of porphyrin crystals, the basis needs to be *extended* to include the second-lowest-frequency normal coordinate of each symmetry. This *extended* basis is also necessary for simulating the IP distortions. The goodness of the simulation can be estimated from the difference between the simulated total distortion (D^{oop}_{sim}, D^{ip}_{sim}) and the observed total distortion (D^{oop}_{obs}, D^{ip}_{obs}), or it can be measured by the mean deviation of the coordinates of each macrocycle atom in the simulated structure from those in the observed structure. The difference between the total deformation of each symmetry obtained from the complete basis and that obtained from the reduced basis (minimal or extended) measures the deviation of the simulation for each symmetry type of deformation. These quantities are mathematically defined elsewhere.[6]

Results

X-ray Crystallography. Figure 3 shows the crystal structures of NiMtBuP and NiDtBuP, respectively. The crystal structure of NiDtBuP has been reported elsewhere,[17] whereas the structure of NiMtBuP was determined for this study. Crystal data, data collection, solution and refinement, atomic coordinates (Ni, C, and N), bond lengths, bond angles, anisotropic displace-

(28) Jentzen, W.; Turowska-Tyrk, I; Scheidt, W. R.; Shelnutt, J. A. *Inorg. Chem.* **1996**, *35*, 3559.
(29) Shelnutt, J. A.; Medforth, C. J.; Berber, M. D.; Barkigia, K. M.; Smith, K. M. *J. Am. Chem. Soc.* **1991**, *113*, 4077.
(30) Mayo, S. L.; Olafson, B. D.; Goddard, W. A., III. *J. Phys. Chem.* **1990**, *94*, 8897.
(31) Li, X.-Y.; Czernuszewics, R. S.; Kincaid, J. R.; Spiro, T. G. *J. Am. Chem. Soc.* **1989**, *111*, 7012. (b) Li, X.-Y.; Czernuszewics, R. S.; Kincaid, J. R.; Su, Y. O.; Spiro, T. G. *J. Phys. Chem.* **1990**, *94*, 31. (c) Li, X.-Y.; Czernuszewics, R. S.; Kincaid, J. R.; Stein, P.; Spiro, T. G. *J. Phys. Chem.* **1990**, *94*, 47.
(32) Cullen, D. L. Meyer, E. F. *J. Am. Chem. Soc.* **1974**, *96*, 2095.
(33) Brennan, T. D.; Scheidt, W. R.; Shelnutt J. A. *J. Am. Chem. Soc.* **1988**, *110*, 3919.
(34) Jentzen, W.; Unger, E.; Song, X.-Z.; Jia, S.-L.; Turowska-Tyrk, I.; Schweitzer-Stenner, R.; Dreybrodt, W.; Scheidt, W. R.; Shelnutt, J. A. *J. Phys. Chem. A* **1997**, *101*, 5789.

Table 1. Selected Average Structural Parameters Obtained from the Calculated Stable Conformers of Nickel Porphine and Mono-, Di-, and Tetra-*tert*-butylporphyrins and Some of Their X-ray Crystal Structures

porphyrin	Ni−N (Å)	dihed angle (deg)	$C_\alpha-N-C_\alpha$ (deg)	N−Ni−N (deg)	$C_\beta-C_\beta$ (Å)	$C_\alpha-C_m$ (Å)	$C_\alpha-N$ (Å)	$N-C_\alpha-C_\beta-C_\beta$ (deg)	$N-C_\alpha-C_m-C_\alpha$ (deg)
NiP									
calcd	1.944	0.1	104.2	180.0	1.330	1.372	1.379	0.0	0.0
X-ray	**1.951**	**1.7**	**104.3**	**179.32**	**1.347**	**1.371**	**1.379**	**0.3**	**0.8**
NiMtBuP									
α	1.914	30.1	105.2	178.0	1.333	1.380	1.377	2.3	13.8
X-ray	**1.901**	**43.9**	**106.3**	**178.9**	**1.342**	**1.380**	**1.380**	**3.0**	**11.1**
NiDtBuP									
αα	1.892	41.4	106.0	175.9	1.334	1.387	1.376	2.0	20.5
X-ray	**1.900**	**46.7**	**106.2**	**177.0**	**1.353**	**1.394**	**1.383**	**2.9**	**14.8**
α*β*	1.928	5.1	104.8	180	1.329	1.383	1.380	5.5	21.2
NiTtBuP									
α*β*α*β*	1.845	56.6	107.7	180	1.336	1.401	1.375	1.6	31.3
αααα	1.931	0.0	104.8	173.0	1.327	1.388	1.382	6.8	37.1
αα*ββ*	1.913	7.6	105.4	180.0	1.329	1.393	1.380	6.7	34.0
ααα*β*	1.882	41.8	106.5	176.4	1.332	1.396	1.378	4.7	32.5

Table 2. Energies (kcal/mol) for the Energy-Optimized Stable Conformers of Nickel Porphine and Mono-, Di-, and Tetra-*meso*-*tert*-butylporphyrins

porphyrin	relative energy	E_{total}	E_{bond}	E_{angle}	$E_{torsion}$	$E_{inversion}$	E_{vdW}	$E_{electrostat}$
NiP		73.05	4.11	70.76	0.00	0.00	11.56	−13.32
NiMtBuP		97.98	6.09	73.59	14.27	0.72	22.35	−19.03
NiDtBuP								
αα	0.00	119.78	9.06	77.11	24.24	0.89	33.26	−24.77
α*β*	10.64	130.42	11.53	80.50	25.76	0.59	36.78	−24.74
NiTtBuP								
α*β*α*β*	0.00	164.36	17.59	85.84	39.36	0.60	56.76	−35.80
αααα	19.54	183.90	18.83	88.53	53.09	0.66	58.51	−35.71
αα*ββ*	21.90	186.26	19.26	89.87	50.55	1.64	60.6	−35.68
ααα*β*	11.87	176.23	17.52	87.74	46.52	1.49	58.76	−35.80

ment parameters, and hydrogen coordinates for NiMtBuP are given in Tables S2−9 (Supporting Information). The atom-labeling scheme is given in Figure S1 (Supporting Information). The crystal and calculated structures are compared in Figure 3. NiDtBuP is found to have the *tert*-butyl substituents in the αα configuration, and the macrocycle shows a gabled (*gab*) conformation.

Molecular Modeling. All the stable conformers (local energy minima) for the series of *tert*-butyl-substituted porphyrins were found by energy minimization of the initially planar structures starting from all meaningful combinations of substituent orientations. The resulting structures are shown (without hydrogen atoms) in Figure 4. Structural parameters for the resulting energy-minimized conformers are listed in Table 1, and the calculated energy distributions for all the conformers are listed in Table 2.

Normal-Coordinate Structural Decomposition. The results of normal-coordinate structural decomposition of each conformer with both the *minimal* and *extended* basis sets are given in Table 3. Table 3 also lists the simulated total distortions and the mean deviations, as well as the total deformation of each symmetry type obtained from NSD using the complete basis set. The simulated structures for the OOP distortion of the macrocycle are shown in "clothesline" displays for the calculated and/or X-ray crystal structures of NiMtBuP in Figure 5, NiDtBuP in Figure S2, and NiTtBuP in Figure 6. In these figures, the black lines represent the actual structures, calculated or X-ray. The blue lines are for the structures as simulated by only the optimal contributions from the lowest-frequency mode deformations. The red lines give the simulated structures obtained using the lowest-frequency and second-lowest-frequency deformations of each out-of-plane symmetry type. The corresponding in-plane distortions are shown in Figures 7, S3, and 8, respectively. Figure 9 graphically illustrates the NSD results for the entire series of porphyrins obtained using the minimal basis.

Spectroscopy. The UV−visible absorption spectra of NiP, NiMtBuP, NiDtBuP and NiTtBuP in CS_2 are shown in Figure S4. With increasing number of substituents, all of the porphyrin absorption bands (B, Q_0, and Q_v) shift to the red and become broader. In addition, the intensity of the Q_0 band becomes weaker relative to the B band and the vibrational sideband Q_v.

The B-band excited resonance Raman spectra of NiP, NiMtBuP, NiDtBuP, and NiTtBuP in CS_2 in the high-frequency and low-frequency regions are shown in Figures 10 and S5, respectively. The frequencies of some of the structure-sensitive lines and other strong lines are listed in Table 4. With increasing number of *tert*-butyl substituents, the structure-sensitive lines such as ν_2, ν_3, and ν_{10} shift to low frequency and ν_8 shifts to higher frequency, indicating an increasing degree of nonplanar distortion.[17,18] The structure-sensitive lines of ν_2 and ν_8 are generally narrow, indicating structural homogeneity[17,18,34] for this series of porphyrins. The doublet of ν_2 for NiDtBuP probably arises from Fermi resonance rather than structural heterogeneity.[17]

Discussion

Conformers of the Nickel *tert*-Butyl-Substituted Porphyrin Series. Not surprisingly, the degree of nonplanarity is found to increase (Tables 1 and 3) as the number of substituents and the van der Waals energy increase (Table 2). NiP is planar (Figure 4a), in agreement with the X-ray crystal structure.[28] The substituted porphyrins are nonplanar. NiMtBuP has only one possible conformer, which is shown in Figure 4b. The calculated structure agrees well with the crystal structure (Figure 3a), except that the ruffling is underestimated by about 0.5 Å (Table 3). NiDtBuP has two possible conformers: the αα

Table 3. Normal-Coordinate Structural Decomposition Results for the X-ray Crystal and Energy-Minimized Structures of the Series of Nickel(II) *meso-tert*-Butyl-Substituted Porphyrins: Displacements (Å) along the Normal Coordinates of Each Symmetry Using the Minimal,[a] Extended,[b] and Complete[c] Basis Sets[d]

	out-of-plane displacements								in-plane displacements							
porphyrin	D_{oop}	$\bar{\delta}_{oop}$	B_{2u}	B_{1u}	A_{2u}	E_{gx}	E_{gy}	A_{1u}	D_{ip}	$\bar{\delta}_{ip}$	B_{2g}	B_{1g}	E_{ux}	E_{uy}	A_{1g}	A_{2g}
NiP																
X-ray																
e	**0.088**	**0.006**	**0.012**	**0.080**	**0.006**	**0.003**	**−0.033**	**−0.003**	**0.158**	**0.008**	**0.007**	**0.010**	**−0.004**	**−0.006**	**−0.157**	**0**
f	*0.094*	*0.002*	*0.013*	*0.080*	*0.006*	*0.003*	*−0.032*	*−0.003*	*0.159*	*0.007*	*0.007*	*0.010*	*−0.004*	*−0.006*	*−0.157*	*0*
f			*0.008*	*0.003*	*−0.005*	*−0.005*	*0.031*	*0*			*−0.007*	*0*	*−0.007*	*−0.005*	*−0.015*	*−0.003*
g	0.094	0	0.015	0.080	0.008	0.009	0.046	0.003	0.164	0	0.010	0.011	0.010	0.011	0.162	0.005
calcd																
	0	**0**	**0**	**0**	**0**	**0**	**0**	**0**	**0.199**	**0.011**	**0**	**0**	**0**	**0**	**−0.199**	**0**
	0	*0*	*0*	*0*	*0*	*0*	*0*	*0*	*0.203*	*0.007*	*0*	*0*	*0*	*0*	*−0.199*	*0*
			0	*0*	*0*	*0*	*0*	*0*			*0*	*0*	*0*	*0*	*−0.040*	*0*
	0	0	0	0	0	0	0	0	0.207	0	0	0	0	0	0.207	0
NiMtBuP																
X-ray																
	2.023	**0.016**	**−0.037**	**1.999**	**0.135**	**0.211**	**0.180**	**−0.002**	**0.572**	**0.051**	**−0.090**	**0.003**	**0.082**	**0.074**	**−0.554**	**−0.007**
	2.025	*0.011*	*−0.037*	*1.999*	*0.131*	*0.210*	*0.179*	*−0.002*	*0.614*	*0.028*	*−0.089*	*0.004*	*0.081*	*0.074*	*−0.553*	*−0.007*
			0.002	*0.020*	*−0.087*	*−0.032*	*−0.032*	*0.010*			*0.033*	*0.023*	*−0.025*	*0.013*	*0.218*	*0*
	2.026	0	0.038	1.999	0.161	0.216	0.190	0.010	0.638	0	0.099	0.034	0.096	0.088	0.616	0.009
calcd																
	1.528	**0.035**	**0**	**1.453**	**0.280**	**0.269**	**0.268**	**0**	**0.484**	**0.026**	**−0.081**	**0**	**0.104**	**0.104**	**−0.454**	**0**
	1.544	*0.023*	*0*	*1.453*	*0.273*	*0.266*	*0.266*	*0*	*0.501*	*0.020*	*−0.081*	*0*	*0.104*	*0.104*	*−0.454*	*0*
			0	*0.113*	*−0.162*	*−0.072*	*−0.072*	*0*			*0.084*	*0*	*−0.018*	*−0.018*	*0.095*	*0*
	1.551	0	0	1.459	0.324	0.295	0.294	0	0.515	0	0.123	0	0.117	0.116	0.472	0
NiDtBuP																
X-ray																
	2.239	**0.033**	**−0.021**	**2.182**	**0.488**	**−0.079**	**0.078**	**0.007**	**0.646**	**0.058**	**−0.261**	**−0.002**	**0.036**	**−0.043**	**−0.588**	**0**
	2.248	*0.008*	*−0.021*	*2.182*	*0.480*	*−0.079*	*0.078*	*0.007*	*0.697*	*0.030*	*−0.261*	*−0.002*	*0.035*	*−0.043*	*−0.587*	*0*
			0.004	*0.062*	*−0.199*	*0.014*	*−0.008*	*0*			*0.112*	*0*	*−0.018*	*0.031*	*0.234*	*−0.003*
	2.249	0	0.021	2.183	0.528	0.081	0.079	0.007	0.721	0.000	0.294	0.004	0.044	0.059	0.655	0.003
αα																
	2.085	**0.054**	**0**	**2.013**	**0.541**	**0**	**0**	**0**	**0.692**	**0.055**	**−0.195**	**0**	**0**	**0**	**−0.664**	**0**
	2.113	*0.014*	*0*	*2.013*	*0.528*	*0*	*0*	*0*	*0.746*	*0.029*	*−0.193*	*0*	*0*	*0*	*−0.663*	*0*
			0	*0.188*	*−0.287*	*0*	*0*	*0*			*0.188*	*0*	*0*	*0*	*0.206*	*0*
	2.114	0	0	2.023	0.615	0	0	0	0.764	0	0.282	0	0	0	0.710	0
α*β*																
	0.985	**0.065**	**0**	**0**	**0**	**0.696**	**0.697**	**0**	**0.378**	**0.018**	**−0.130**	**0**	**0**	**0**	**−0.355**	**0**
	1.020	*0.056*	*0*	*0*	*0*	*0.689*	*0.690*	*0*	*0.384*	*0.013*	*−0.129*	*0*	*0*	*0*	*−0.355*	*0*
			0	*0*	*0*	*−0.187*	*−0.188*	*0*			*0.057*	*0*	*0*	*0*	*−0.039*	*0*
	1.074	0	0	0	0	0.759	0.759	0	0.391	0	0.147	0	0	0	0.362	0
NiTtBuP																
α*β*α*β*																
	2.744	**0.059**	**0**	**2.744**	**0**	**0**	**0**	**0**	**0.986**	**0.090**	**0**	**0**	**0**	**0**	**−0.986**	**0**
	2.763	*0.018*	*0*	*2.744*	*0*	*0*	*0*	*0*	*1.096*	*0.039*	*0*	*0*	*0*	*0*	*−0.985*	*0*
			0	*0.322*	*0*	*0*	*0*	*0*			*0*	*0*	*0*	*0*	*0.478*	*0*
	2.765	0	0	2.765	0	0	0	0	1.117	0	0	0	0	0	1.117	0
αααα																
	1.195	**0.122**	**0**	**0**	**1.195**	**0**	**0**	**0**	**0.495**	**0.047**	**0**	**0**	**0**	**0**	**−0.495**	**0**
	1.448	*0.026*	*0*	*0*	*1.160*	*0*	*0*	*0*	*0.528*	*0.030*	*0*	*0*	*0*	*0*	*−0.495*	*0*
			0	*0*	*−0.818*	*0*	*0*	*0*			*0*	*0*	*0*	*0*	*−0.185*	*0*
	1.455	0	0	0	1.455	0	0	0	0.549	0	0	0	0	0	0.549	0
αα*ββ*																
	1.433	**0.084**	**0**	**0**	**0**	**1.433**	**0**	**0**	**0.556**	**0.033**	**0**	**−0.191**	**0**	**0**	**−0.522**	**0**
	1.473	*0.074*	*0*	*0*	*0*	*1.420*	*0*	*0*	*0.560*	*0.029*	*0*	*−0.191*	*0*	*0*	*−0.522*	*0*
			0	*0*	*0*	*−0.341*	*0*	*0*			*0*	*−0.046*	*0*	*0*	*−0.047*	*0*
	1.543	0	0	0	0	1.543	0	0	0.583	0	0	0.229	0	0	0.536	0
ααα*β*																
	2.269	**0.076**	**0**	**−2.007**	**0.601**	**0.616**	**0.617**	**0**	**0.845**	**0.086**	**0.014**	**0**	**−0.187**	**−0.187**	**−0.803**	**0**
	2.303	*0.049*	*0*	*−2.007*	*0.586*	*0.613*	*0.613*	*0*	*0.927*	*0.054*	*0.013*	*0*	*−0.184*	*−0.184*	*−0.802*	*0*
			0	*−0.164*	*−0.333*	*−0.097*	*−0.097*	*0*			*−0.196*	*0*	*0.197*	*0.197*	*0.173*	*0*
	2.322	0	0	2.014	0.689	0.655	0.655	0	0.977	0	0.213	0	0.316	0.316	0.843	0

[a] Boldface roman. [b] Lightface italic. [c] Lightface roman. [d] The simulated total distortions, D_{oop} and D_{ip} (Å), and the mean deviations, $\bar{\delta}_{oop}$ and $\bar{\delta}_{ip}$ (Å), for different basis sets are also given. The *observed* total distortions are the same as D_{oop} and D_{ip} for the complete basis. [e] Minimal basis: displacements along the lowest-frequency normal coordinate of each symmetry, which are listed in the order of increasing frequency [B_{2u} *sad*, B_{1u} *ruf*, A_{2u} *dom*, E_{gx} *wav*(*x*), E_{gy} *wav*(*y*), and A_{1u} *pro* for out-of-plane; B_{2g} *m-str*, B_{1g} *N-str*, E_{ux} *trn*(*x*), E_{uy} *trn*(*y*), A_{1g} *bre*, and A_{2g} *rot* for in-plane]. [f] Extended basis: the first row in italics lists displacements along the lowest-frequency normal coordinate of each symmetry, and the second row in italics lists the displacements along the second-lowest-frequency normal coordinate of each symmetry. [g] Complete basis: the total deformation of each symmetry as defined in ref 6. The total distortion, D_{oop} and D_{ip}, simulated with the complete basis is equal to the observed total distortion D_{obs}.

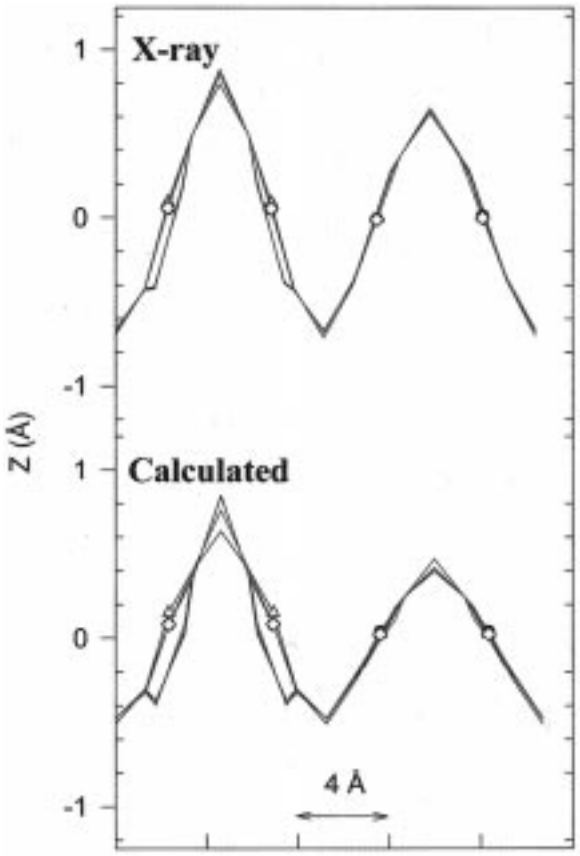

Figure 5. Comparison of the simulated out-of-plane distortions using the minimal basis (blue) and the extended basis (red) with the observed distortion (black) of the macrocyclic atoms for the X-ray crystal structure (top) and the energy-minimized structure (bottom) of NiMt-BuP.

conformer, for which the two substituents are above the average plane of the macrocycle, and the $\alpha\beta$ conformer, for which one substituent is above and the other below the plane. These two conformers are shown in Figure 4, parts c and d. The $\alpha\alpha$ conformer has a *gab* conformation and is more stable by 10 kcal/mol than the $\alpha\beta$ conformer (see Table 2), and thus only the $\alpha\alpha$ conformer exists in solution. Furthermore, the crystal structure of NiDtBuP shows a *gab* conformation and agrees well with the calculated $\alpha\alpha$ conformer (Figure 3b).

With the improved force field, four stable conformers for NiTtBuP, resulting from different orientations of substituents, are predicted as shown in Figure 4, parts e−h: the $\alpha\beta\alpha\beta$ conformer (the four substituents are alternately above and below the average plane), the $\alpha\alpha\alpha\alpha$ conformer (all four substituents are above the plane), the $\alpha\alpha\beta\beta$ conformer (two adjacent substituents are above and the other two are below the plane), and the $\alpha\alpha\alpha\beta$ conformer (three substituents are above and one is below the plane), respectively. The $\alpha\alpha\alpha\beta$ conformer was not stable with the old force field, converting to the $\alpha\beta\alpha\beta$ conformer during energy optimization.[18] The ruffled $\alpha\beta\alpha\beta$ is the most stable, with the other three conformers being 11−22 kcal/mol higher in energy (see Table 2) and unlikely to be significantly populated in solution. The $\alpha\alpha\alpha\alpha$ and $\alpha\alpha\beta\beta$ conformers show purely *dom* and *wav*(*x*) macrocyclic shapes, respectively. The shape of the $\alpha\alpha\alpha\beta$ conformer is a combination of normal deformations.

Distortion along the Lowest-Frequency Normal Coordinates. By examining the NSD results for the series of nickel porphyrins given in Table 3 and Figure 9, one concludes that the distortions of porphyrins occur primarily along the lowest-

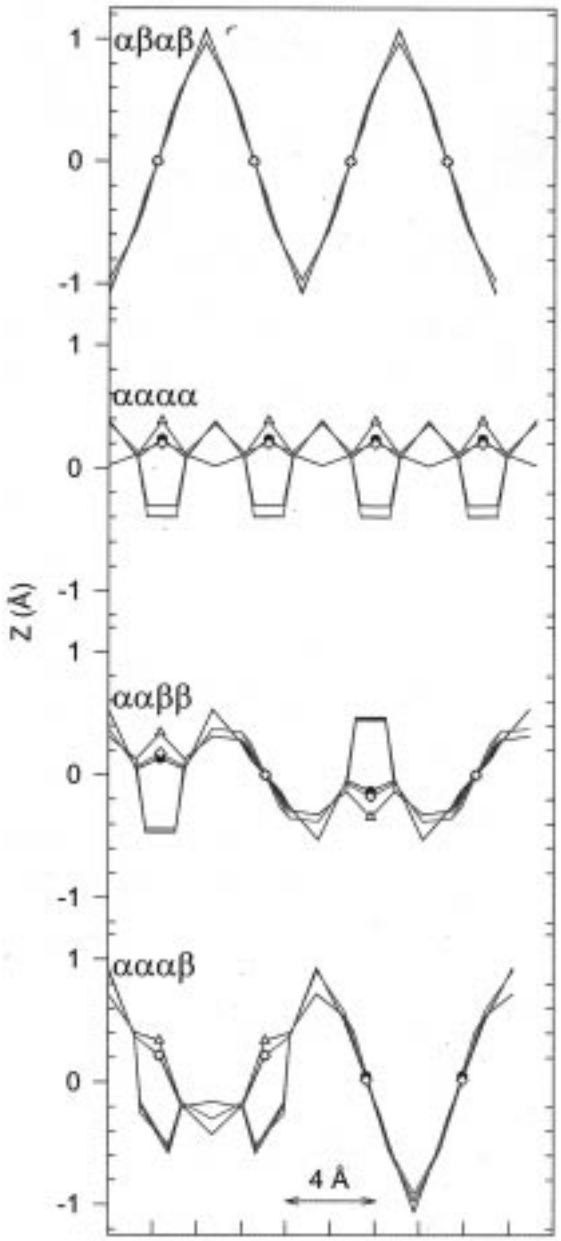

Figure 6. Comparison of the simulated out-of-plane distortions using the minimal basis (blue) and the extended basis (red) with the distortions (black) of the macrocyclic atoms for the energy-minimized stable $\alpha\beta\alpha\beta$, $\alpha\alpha\alpha\alpha$, $\alpha\alpha\beta\beta$, and $\alpha\alpha\alpha\beta$ conformers of NiTtBuP.

frequency normal coordinates of the macrocycle. In particular, the simulated out-of-plane and in-plane total distortions using the minimal basis account for most of the observed total distortions (D_{oop} and D_{ip} in Table 3 obtained using the complete basis). In addition, the displacement along each lowest-frequency normal coordinate accounts for most of the total deformation of each symmetry type. Moreover, displacements along the second-lowest-frequency normal coordinates are much smaller than the displacements along the lowest-frequency ones, especially for the out-of-plane deformations. Nevertheless, the extended basis significantly improves the agreement between the simulated and observed (X-ray and calculated) structures. This is clearly illustrated by the comparison of the simulated structures with the observed structures in the clothesline displays of Figures 5, 6, and S2. While the simulated structure using the minimal basis reflects the main characteristics of the macrocycle distortion for the low-energy conformers, the

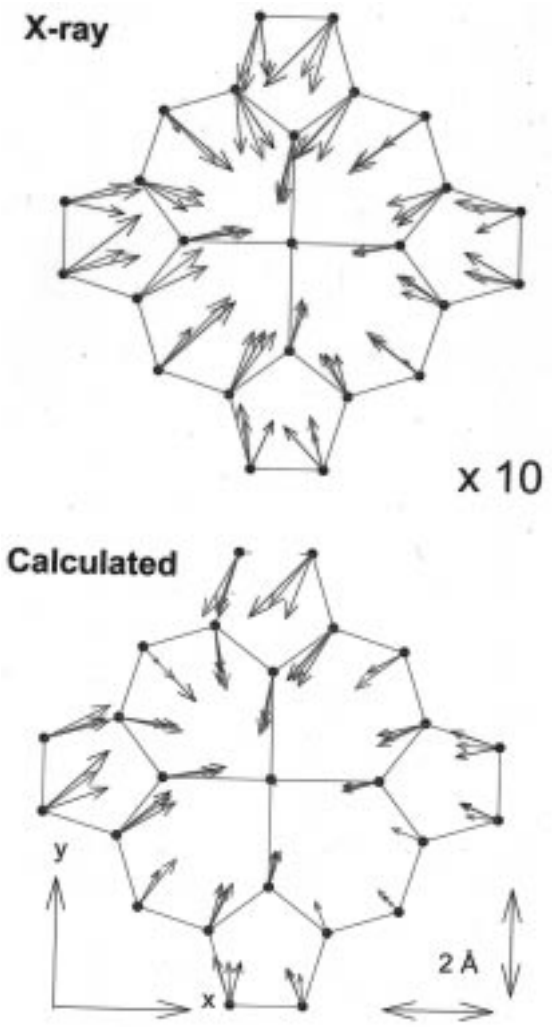

Figure 7. Comparison of the simulated in-plane distortions using the minimal basis (blue) and the extended basis (red) with the observed distortions (black) of the macrocyclic atoms for the X-ray crystal structure (top) and the energy-minimized structure (bottom) of NiMtBuP. The distortions are enlarged by a factor of 10.

extended basis is especially necessary for the high-energy stable structures. For the in-plane distortions in particular, the deformations along the higher-frequency normal coordinates are often significant. That is, displacements along the second-lowest-frequency normal coordinates are usually of a magnitude similar to the displacements along the lowest-frequency coordinates (Table 3). However, expansion of the basis set to also include the second-lowest-frequency modes is adequate, that is, still more high-frequency modes are not required to simulate the structure to within the experimental error. This is verified by comparison of the observed and simulated IP distortions using different basis sets in Figures 7, 8, and S3.

Two main factors cause the large deviations between the simulated and observed structures for the IP distortion when using only the minimal basis of normal modes. The first is the small difference in frequencies of the lowest-frequency and second-lowest-frequency in-plane normal modes of each symmetry. The second-lowest-frequency in-plane normal modes ($A_{1g}^{(2)}$, $A_{2g}^{(2)}$, $B_{1g}^{(2)}$, $B_{2g}^{(2)}$, and $E_u^{(2)}$) are calculated to be at 701 cm^{-1} (1.9 $A_{1g}^{(1)}$), 769 cm^{-1} (1.4 $A_{2g}^{(1)}$), 757 cm^{-1} (2.9 $B_{1g}^{(1)}$), 428 cm^{-1} (2.0 $B_{2g}^{(1)}$), and 413 cm^{-1} (1.1 $E_u^{(1)}$), respectively. This is in contrast with the second-lowest-frequency out-of-plane normal modes ($A_{1u}^{(2)}$, $A_{2u}^{(2)}$, $B_{1u}^{(2)}$, $B_{2u}^{(2)}$, and $E_g^{(2)}$), calculated to be at 680 cm^{-1} (2.0 $A_{1u}^{(1)}$), 359 cm^{-1} (2.7 $A_{2u}^{(1)}$), 516 cm^{-1} (5.9 $B_{1u}^{(1)}$), 721 cm^{-1} (11.1 $B_{2u}^{(1)}$), and 238 cm^{-1} (1.4 $E_g^{(1)}$), respectively.[6] Thus, the frequency ratios are generally closer to unity (i.e., the modes are more energetically equivalent) for the in-plane symmetries than for the out-of-plane symmetries. Another factor is that the number of degrees of freedom within each symmetry type is higher for the IP modes than for the OOP modes. That is, the number of modes of each in-plane symmetry (6 A_{1g}, 5 A_{2g}, 6 B_{1g}, 6 B_{2g}, 11 E_g) is larger than for the out-of-plane symmetries (2 A_{1u}, 3 A_{2u}, 3 B_{1u}, 3 B_{2u}, 5 E_g). Thus, small contributions from a number of modes may contribute to the distortion.

These two factors also account for the frequently observed larger deviations between simulated and observed structures for the *dom* and *wav* OOP deformations than for the *ruf* type when using the minimal basis. This effect can be seen for the NSD results for the calculated NiTtBuP conformers (Table 3). NSD shows that the distortion of the $\alpha\beta\alpha\beta$ conformer is purely B_{1u}, that of the $\alpha\alpha\alpha\alpha$ conformer is purely A_{2u}, and that of the $\alpha\alpha\beta\beta$ conformer is purely E_{gx}. However, because of the large frequency ratio for B_{1u} symmetry and small frequency ratios for A_{2u} and E_g symmetries, the minimal basis accurately simulates the nonplanar distortion of the $\alpha\beta\alpha\beta$ conformer, but only approximately simulates the distortions of the $\alpha\alpha\alpha\alpha$ and $\alpha\alpha\beta\beta$ conformers as shown in Figure 6. Consequently, the extended basis set is needed to accurately simulate the distortions of the $\alpha\alpha\alpha\alpha$ and $\alpha\alpha\beta\beta$ conformers. Because of the large number of degrees of freedom for E_g symmetry, an obvious deviation still exists even with the extended basis (Figure 6). When the third-lowest-frequency normal coordinates of E_g symmetry are included in the basis, there is no significant deviation between the simulated and observed structures for the $\alpha\alpha\beta\beta$ conformer (results not shown). Finally, it is interesting to note that, because of the (near) orthogonality of the normal deformations, the projection along one coordinate is (almost) independent of the size of the basis set (minimal, extended, or complete).

Relationship between the Type of Out-of-Plane and In-Plane Distortions and the Perturbation Symmetry. The NSD results in Table 3 and Figure 9 show that different substituent conformations give different types of out-of-plane and in-plane deformations. For example, in terms of the minimal basis set, the $\alpha\beta\alpha\beta$ conformer of NiTtBuP is purely *ruf* (B_{1u}) for the OOP deformation and purely *bre* (A_{1g}) for the IP deformation; the $\alpha\alpha\alpha\alpha$ conformer is purely *dom* (A_{2u}) for OOP and purely *bre* for IP; the $\alpha\alpha\beta\beta$ conformer is purely *wav*(*x*) (E_{gx}) for OOP and a linear combination of *bre* and *N-str* (B_{1g}) for IP; and the $\alpha\alpha\alpha\beta$ conformer is a linear combination of *ruf*, *dom*, *wav*(*x*), and *wav*(*y*) (E_{gy}) for OOP and a linear combination of *m-str* (B_{2g}), *trn*(*x*) (E_{ux}), *trn*(*y*) (E_{uy}), and *bre* for IP. The deformations that arise are related to the perturbation symmetry of the peripheral substituents.

For the *tert*-butyl-substituted porphyrins, the possible orientations of the substituents (Figure 11) are known beforehand because of the simple shape of the *tert*-butyl group. For a planar macrocycle, each *tert*-butyl group can have only two possible orientations with respect to the macrocycle. The repulsive van der Waals interaction ensures that one of its methyl groups will orient vertically and that this vertical plane will bisect the other two methyls. This is the optimal way to relieve the steric strain for the *tert*-butyl group. The two orientations come from the up or down orientation of the vertical methyl group. This up/down orientation of the substituents is illustrated by the wedge-shaped (solid, dashed) bonds in Figure 11. In the series of nickel porphyrins with different numbers and orientations of *meso*-

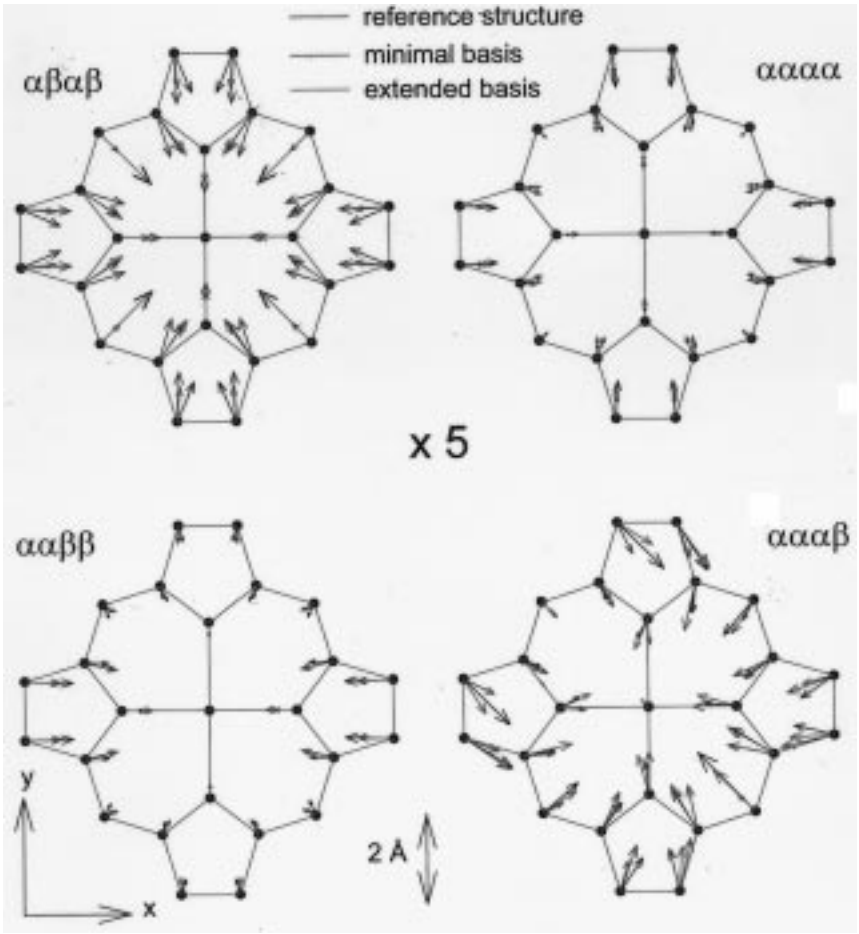

Figure 8. Comparison of the simulated in-plane distortions using the minimal (blue) and extended (red) basis with the distortions (black) for the energy-minimized conformers of NiTtBuP. The distortions are enlarged by a factor of 5.

tert-butyl substituents illustrated in Figure 11, each conformer has a specific type of perturbation symmetry in D_{4h}. Figure 11 indicates these perturbation symmetries for this series of porphyrins. The symmetric perturbation causes the macrocycle to distort only with certain types of deformations.

Each molecular symmetry that is illustrated in Figure 11 allows only certain types of deformations from the D_{4h} group representations. The symmetry-allowed deformations belong to those irreducible representations of the D_{4h} point group that are totally symmetric in the molecular point group of lower symmetry. These allowed symmetry types are easily determined from a correlation table for the D_{4h} point group (Table S1). For example, the perturbation of the $\alpha\beta\alpha\beta$ orientation of NiTtBuP has symmetry belonging to the $D_{2d}(C'_2)$ point group Figure 11e). From the correlation table, the A_{1g} and B_{1u} representations in the D_{4h} point group are totally symmetric A_1 representations in the $D_{2d}(C'_2)$ point group. Thus, the symmetrically allowed deformations for $\alpha\beta\alpha\beta$-NiTtBuP are A_{1g} for IP and B_{1u} for OOP deformations. Consequently, the resulting deformations are mainly *ruf* (B_{1u}) and *bre* (A_{1g}) for the $\alpha\beta\alpha\beta$ conformer. These deformations give the familiar ruffling of the macrocycle and associated contraction of the porphinato core.

Similarly, the C_{4v} symmetry of the $\alpha\alpha\alpha\alpha$ orientation allows A_{2u} symmetry for OOP and A_{1g} symmetry for IP deformations, resulting in the familiar domed conformation. $C_{2h}(C'_2)$ symmetry of the $\alpha\alpha\beta\beta$ orientation gives E_g for OOP and A_{1g} and B_{1g} symmetries for IP deformations. The resulting conformers have primarily a *wav* OOP deformation and an IP *N-str* deformation. Finally, the $C_s(S_d)$ symmetry of the $\alpha\alpha\alpha\beta$ substituent orientation allows B_{1u}, A_{2u}, and E_g symmetries for OOP and A_{1g}, B_{2g}, and E_u IP symmetries. These results agree precisely with the NSD results shown in Table 3 (and Figure 9). Thus, as expected, a simple relationship exists between the types of deformation and the perturbation symmetry. That is, if the orientations of the substituents for the planar macrocycle can be predicted without molecular mechanics, then the contributing normal deformations can be known beforehand.

If the substituent pattern lowers the symmetry, that is, there are fewer than four meso substituents, then additional normal deformations will contribute to the distortion. For example, for NiMtBuP there is only the one meso substituent. When the substituent orientation relative to the macrocycle plane is considered, it produces a perturbation with $C_s(S_d)$ symmetry (Figure 11b). From the correlation table, the A_{1g}, B_{1g}, E_u, B_{1u}, A_{2u}, and E_g representations in the D_{4h} point group transform like A′ in the $C_s(S_d)$ point group. Thus, the OOP deformations are primarily *ruf*, *dom*, *wav*(*x*), and *wav*(*y*), and the IP deformations are *bre*, *N-str*, *trn*(*x*), and *trn*(*y*). This is confirmed by the decomposition results in Table 3 and Figure 9, which shows that OOP deformations of A_{1u} and B_{2u} symmetries are missing, and B_{1g} and A_{2g} IP symmetries are missing.

For the NiDtBuP, two combinations of substituent orientations labeled as $\alpha\alpha$ and $\alpha\beta$ are possible (Figure 11c, and d). The $\alpha\alpha$ orientation gives $C_{2v}(C_2,S_d)$ symmetry, and the $\alpha\beta$ orientation gives $C_{2h}(C''_2)$ symmetry. Again, from the correlation table, the symmetry-allowed types of deformations are of A_{1g}, B_{2g}, A_{2u}, and B_{1u} symmetries for $C_{2v}(C_2,S_d)$ and of A_{1g}, B_{2g}, and E_g symmetries for $C_{2h}(C''_2)$. Consequently, the nonplanar distortion of the $\alpha\alpha$ conformer is mainly composed of *ruf* (B_{1u}) and *dom*

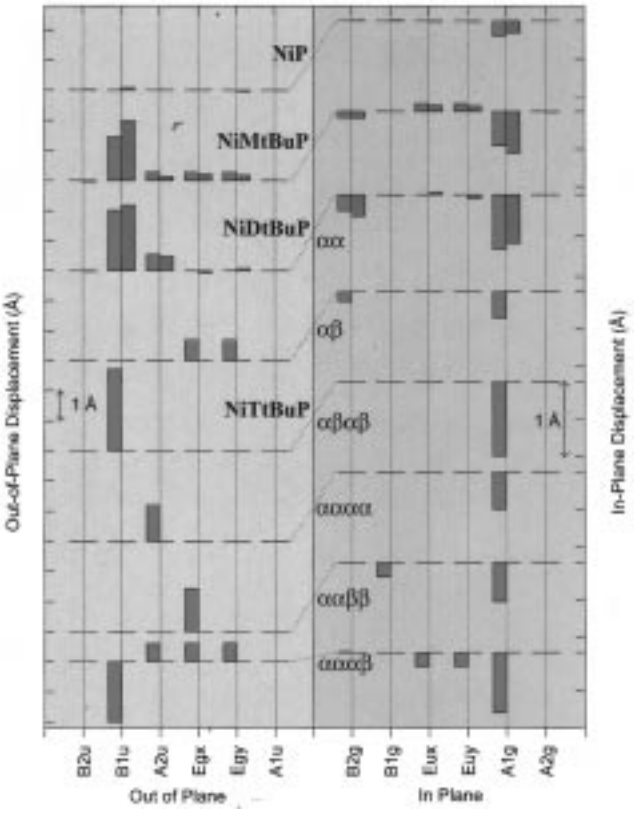

Figure 9. Graphical representations of the displacements along the lowest-frequency coordinates that best simulate the structures of the series of nickel porphyrins: cyan, X-ray structure; red, calculated structure.

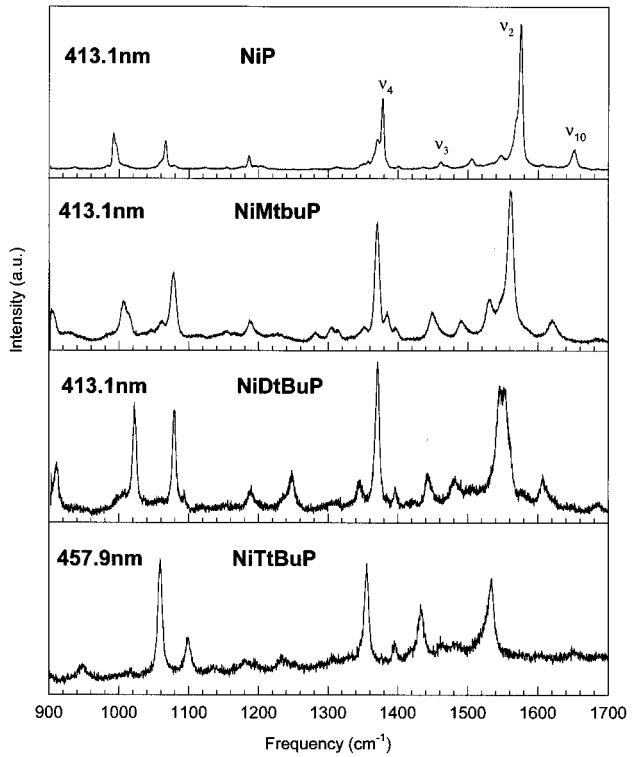

Figure 10. High-frequency region of the resonance Raman spectra of NiP, NiMtBuP, NiDtBuP, and NiTtBuP in carbon disulfide.

(A_{2u}) deformations, and the $\alpha\beta$ conformers is composed of equal *wav*(*x*) and *wav*(*y*) (E_{gx} and E_{gy}) deformations. The in-plane distortions of the $\alpha\alpha$ and $\alpha\beta$ conformers are the same, a linear combination of *bre* (A_{1g}) and *m-str* (B_{2g}) deformations.

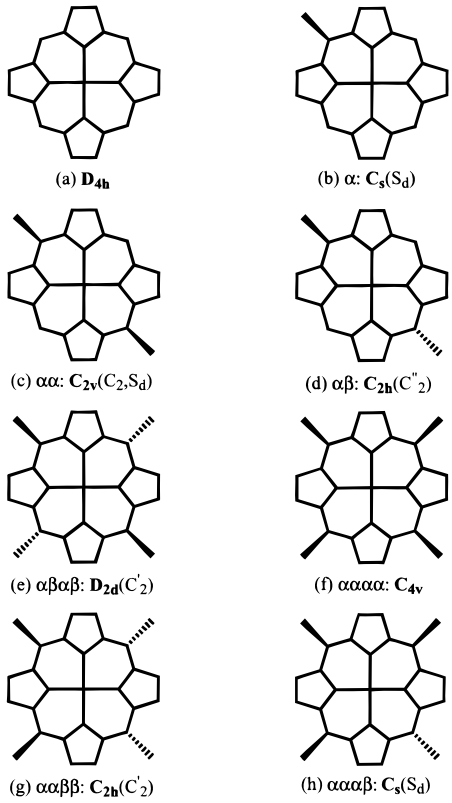

Figure 11. Perturbation symmetries from different patterns of peripheral substitution and orientations of substituents for the series of nickel *meso-tert*-butyl-substituted porphyrins.

Table 4. Frequencies (cm^{-1}) of Selected Resonance Raman Lines for the Series Consisting of Nickel(II) Porphine and Mono-, Di-, and Tetra-*tert*-butylporphyrins in CS_2

Raman line	NiP	NiMtBuP	NiDtBuP	NiTtBuP
ν_2	1575	1561	1548	1533
ν_3	1461	1449	1443	1433
ν_4	1378	1370	1371	1355
ν_9	1067	1078	1079	1098
ν_6	992	1007	1023	1059
ν_8	369	379	398	418

Macrocycle Distortion in Crystal Structures. The types of distortion are mainly those symmetrically allowed by the substituent perturbation symmetry; however, crystal-packing forces may alter allowed deformations or introduce other symmetry types. From the NSD results for the X-ray crystal structure for NiMtBuP (Table 3 and Figure 9), the main types of deformations are *ruf* (B_{1u}), *dom* (A_{2u}), *wav*(*x*) (E_{gx}), and *wav*(*y*) (E_{gy}) for OOP and *bre* (A_{1g}), *m-str* (B_{2g}), *trn*(*x*) (E_{ux}), and *trn*(*y*) (E_{uy}) deformations for IP. These are the symmetries predicted from the maximum perturbation symmetry of the substituents. However, the small contribution from the *sad* deformation may be caused by crystal packing. In addition, the inequality of *wav*(*x*) and *wav*(*y*) deformations may also result from crystal-packing effects. The small contributions from *pro* (A_{1u}), *N-str* (B_{1g}), and *rot* (A_{2g}) deformations are most likely a result of the random errors in the X-ray crystal structure. From the NSD results for the X-ray crystal structure of NiP, the small amounts of *ruf*, *wav*(*y*), *sad*, and *N-str* deformations may be caused by crystal packing, including Ni interaction with a nitrogen of a neighboring porphyrin macrocycle.[28]

If the substituents of a porphyrin have more than one possible combination of orientations, then the conformation that occurs in the crystal depends on the relative energies of the conformers. If the energy differences are small, several conformations may

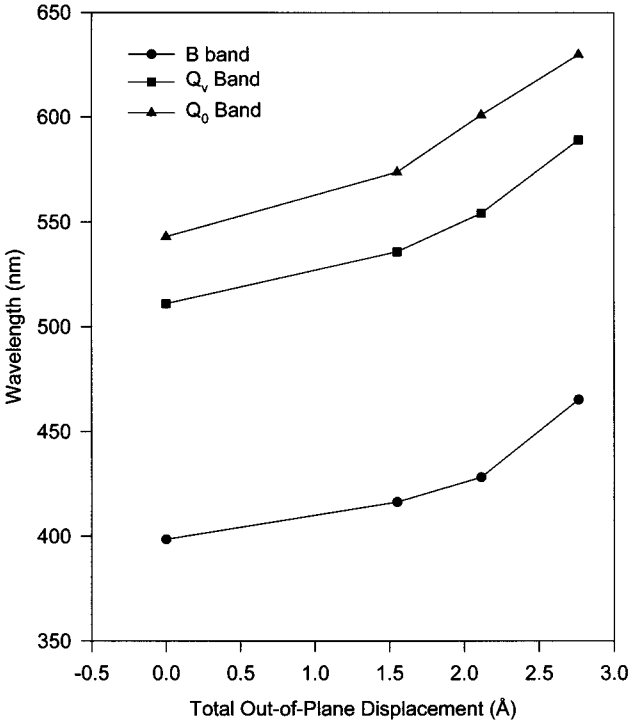

Figure 12. Correlation between the absorption maxima and total out-of-plane displacements for the series of nickel *meso-tert*-butyl-substituted porphyrins.

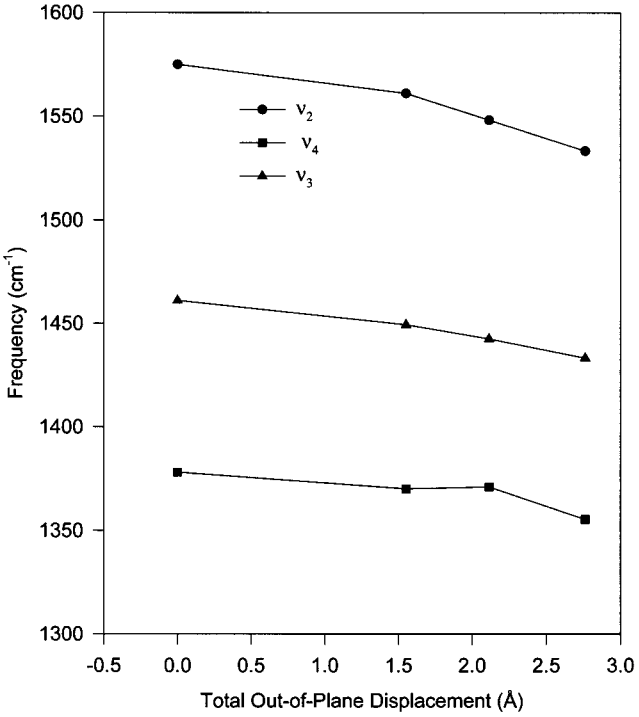

Figure 13. Correlation between the frequencies of some structure-sensitive Raman lines and the total out-of-plane displacements for the series of nickel *meso-tert*-butyl-substituted porphyrins.

be observed in the crystalline state. For nickel octaethylporphyrin (NiOEP), the energy differences between stable conformers with different ethyl orientations are calculated to be less than 2 kcal/mol,[35] and triclinic A,[32] triclinic B,[33] and tetragonal[36] crystalline forms of NiOEP have different substituent orientations. On the other hand, if energy differences among different stable conformers are large, the conformation observed in the crystal is likely the most stable one. For example, NiDtBuP has two stable conformers ($\alpha\alpha$ and $\alpha\beta$), but because the energy of the $\alpha\beta$ conformer is much higher (10.64 kcal/mol, Table 2) than that of the $\alpha\alpha$ conformer, only the $\alpha\alpha$ conformation is predicted and observed in the crystal (Figure 3b). Further, the main types of distortions in the crystal are *ruf* and *dom* deformations for OOP and *bre* and *m-str* deformations for IP, as predicted from the $\alpha\alpha$ substituent perturbation symmetry. Crystal-packing forces likely cause the small out-of-plane *wav*(*x*), *wav*(*y*), and *sad* deformations and the small in-plane *trn*(*x*) and *trn*(*y*) deformations (Figure 9).

The Degree of Nonplanar Distortions. For the series of nickel *meso-tert*-butyl-substituted porphyrins, only one conformer (the most stable one) exists in solution for each porphyrin (see Table 2). These conformers are the planar conformer of NiP, the α conformer of NiMtBuP, the $\alpha\alpha$ conformer of NiDtBuP, and the $\alpha\beta\alpha\beta$ conformer of NiTtBuP. MM calculations and X-ray crystallography show that the total degree of nonplanarity, as characterized by the total root-squares out-of-plane displacement of the 24 macrocycle atoms, increases as the number of *meso-tert*-butyl substituents increases (Table 3). This is confirmed by the UV−visible and resonance Raman spectra of these porphyrins. Figure 12 shows the peak positions of the absorption bands B, Q_v, and Q_0 in carbon disulfide solutions as a function of the total out-of-plane displacement for NiP, α-NiMtBu, $\alpha\alpha$-NiDtBuP, and $\alpha\beta\alpha\beta$-NiTtBuP. The wavelengths of all the absorption bands increase in a nonlinear way, as the porphyrin becomes more nonplanar. INDO/s calculations show that the red shifts are caused by nonplanar distortions of the porphyrin macrocycle (Song, X.-Z., unpublished results).

Nonplanar distortion of the macrocycle is known to cause downshifts in the frequencies of the structure-sensitive lines, especially ν_2, ν_3, and ν_{10}.[17,18,28,37] The dependence on the total OOP displacement of the structure-sensitive Raman lines, ν_2 and ν_3, and the oxidation-state marker line ν_4 is shown in Figure 13. The observed downshifts of ν_2 and ν_3 are completely consistent with the MM predictions and crystal structures which show the macrocycle becoming more nonplanar as the number of *tert*-butyl substituents increases.

Conclusions

The distortion of a metalloporphyrin that is induced by peripheral substitution occurs mainly along the lowest-frequency normal coordinates of the macrocycle. The types of out-of-plane and in-plane deformations present for a conformer are primarily determined by the perturbation symmetry of the substituents, especially if the steric interaction between the macrocycle and substituents is large. The perturbation symmetry is determined by the pattern of substitution and the orientations of the substituents. Hence, given a substituted metalloporphyrin, the main types of deformations present in the stable conformers can usually be predicted from the perturbation symmetry of the substituents alone. Molecular mechanics calculations are needed to determine the magnitudes of these symmetric deformations. The relative energies of the stable

(35) Jia, S.-L.; Shelnutt, J. A., unpublished results.
(36) Meyer, E. F. *Acta Crystallogr., Sect. B* **1972**, *28*, 2162.
(37) Czernuszewicz, R. S.; Li, X.-Y.; Spiro, T. G. *J. Am. Chem. Soc.* **1989**, *111*, 7024. (b) Prendergast, K.; Spiro, T. G. *J. Am. Chem. Soc.* **1992**, *114*, 3793.

conformers, also provided by MM calculations, predict which conformers may appear in crystals and in solution.

From another point of view, the types of deformations present in a porphyrin report upon the symmetry of the "external" perturbation. Thus, structural analysis of the macrocycle in porphyrin-containing proteins can provide insights into the symmetry of the protein-induced perturbation. Therefore, the types and magnitudes of the deformations of porphyrins in proteins can be used to probe the properties of the protein environment at the active site.

Acknowledgment. Work performed at the University of California at Davis was supported by grants from the National Science Foundation (CHE-93-05577) and the National Institutes of Health (HL-22252) (K.M.S.).

Supporting Information Available: A symmetry correlation table for the D_{4h} point group and its subgroups (Table S1), the X-ray crystal structure data for NiMtBuP (Tables S2−9), the atom-labeling scheme for the X-ray crystal structure of NiMtBuP (Figure S1), comparison of the simulated structure using the minimal and extended bases with the observed structures for the X-ray crystal structure and energy-minimized stable conformers of NiDtBuP (Figure S2), comparison of the simulated in-plane distortions using the minimal and extended bases to the observed distortions for the X-ray crystal structure and energy-minimized stable conformers of NiDtBuP (Figure 3S), the UV−visible absorption spectra of NiP, NiMtBuP, NiDtBuP, and NiTtBuP in carbon disulfide (Figure S4), and the resonance Raman spectra of NiP, NiMtBuP, NiDtBuP and NiTtBuP in carbon disulfide in the low-frequency region (Figure S5) (20 pages). Ordering information is given on any current masthead page.

IC9711978